Elastic Rescattering in the Strong Field Tunneling Limit

B. Walker,[1] B. Sheehy,[1] K. C. Kulander,[2] and L. F. DiMauro[1]
[1]*Chemistry Department, Brookhaven National Laboratory, Upton, New York 11973*
[2]*TAMP, Lawrence Livermore National Laboratory, Livermore, California 94551*
(Received 8 August 1996)

High precision measurements of helium photoelectron energy and angular distributions for a broad intensity range reflect the change in the continuum dynamics that occurs as the ionization process evolves into the pure tunneling regime. Elastic rescattering of the laser-driven free electron from its parent ion core leaves a distinct signature on the spectra, providing a direct quantitative test of the various theories of strong field multiphoton ionization. We show that it takes a relatively complete semiclassical rescattering model to accurately reproduce the observed distributions. [S0031-9007(96)01922-9]

PACS numbers: 32.80.Rm, 31.90.+s, 32.80.Fb

Strong field photoelectron spectra have attracted considerable attention over the past decade and a half, but a comprehensive understanding of the underlying dynamics which produce these spectra and related phenomena has solidified with the development of high repetition-rate, short pulse lasers which can span the entire intensity range of importance [1]. Keldysh [2] showed that at infrared and visible wavelengths the dynamics of strong field atomic ionization undergoes a change in character as the laser intensity increases. In weak fields electrons are promoted into the continuum by the simultaneous absorption of enough photons to increase their energy above the ionization potential. This is called multiphoton ionization (MPI). However, as the laser intensity increases, a completely separate mode of escape becomes possible. At large distances from the nucleus, the electrostatic attraction of the ion core can be overwhelmed by the laser's instantaneous electric field, producing a barrier through which a valence electron can tunnel. In this regime a quasistatic tunneling picture becomes appropriate: the laser field varies so slowly compared to the response time of the electron that the ionization rate becomes simply the cycle average of the instantaneous dc tunneling rate. Tunneling becomes important when the ratio of the frequency of the applied field to the tunneling rate becomes smaller than unity. This ratio, known as the Keldysh or adiabaticity parameter, γ, is given by $\sqrt{I_p/(2U_p)}$, where I_p is the binding energy of the electron and $U_p = I/4\omega^2$ is the ponderomotive energy in atomic units of a free electron in the laser field of frequency ω and intensity I.

The majority of experimental studies on neutral atoms exposed to intense, short–pulse laser fields have been carried out in the MPI regime ($\gamma \geq 1$). A few experiments [3–6] have extended into the tunneling regime, but these measurements have been limited to observations of total ionization rates or electron energy distributions over a small dynamic range. In this Letter, we report upon the first systematic experimental investigation in the strong field tunneling limit. Our study, by virtue of the enhanced dynamic range accessible with kilohertz laser technology, follows the change in the electron spectrum and angular distributions as the ionization evolves from predominantly MPI to pure tunneling. We find that the electron distributions in the tunneling regime are very different from any previous reports obtained in the MPI or mixed regimes [7–9]. We achieve a quantitative description of these spectra using a rescattering picture [9,10] which mimics the time evolution of a tunnel-ionized continuum wave packet in the *combined* fields of the laser and ion core. Since rescattering events are known to be important in other short-pulse, strong-field emission phenomena (e.g., harmonic generation), this investigation better defines the underlying dynamics of these processes.

In the experiments presented here, a 150 fs, 1 kHz repetition rate, titanium sapphire laser operating at 0.78 μm was focused by $f/4$ optics into an ultrahigh vacuum chamber, producing a maximum intensity of 20 PW/cm^2. The sample gas was 99.999% helium, which was further scrubbed to <0.1 ppm for O_2, H_2, H_2O, CO_2, and hydrocarbon impurities. A 30 cm long time-of-flight photoelectron (PE) spectrometer provides energy and angular resolution of 0.05 eV and 65 mrad, respectively. Data collection used 1 ns binning of discriminated electron events operating at low event probability ($\leq$0.25/shot), ensuring space charge free conditions. The spectrometer's energy calibration was obtained by recording the high order (>40 photon absorption), long pulse above-threshold ionization spectrum of xenon. The intensity was calibrated using measurements of the total ion yield, xenon short-pulse PES resonances, and spot size [11]. The uncertainty in the reported intensities is $\sim$25%. The current PE spectra were recorded between 0.5 and 1.5 times the saturation intensity ($I_{\text{sat}} = 0.8$ PW/cm^2) for neutral helium. Walker *et al.* [11] showed that contributions due to sequential ionization of He^+ remain insignificant up to an intensity of $\sim$4 PW/cm^2. A small fraction of the PE's are produced via direct double ionization. It is not clear what the spectral characteristics of these electrons are, but their low abundance probably precludes their observation without some sort of coincidence measurement.

Our recent ion and electron measurements [11] have confirmed that helium tunnel ionizes near saturation. This was established by comparing experimental helium ion yield curves with calculations using time-dependent quantum mechanical (total) and ac-tunneling rates. The ratio of the tunneling rate to the total rate for the intensities of 0.4, 0.8, and 1.2 PW/cm^2 used in this study are 0.7, 1.0, and 1.0, respectively. Therefore, helium ionization has some MPI component at the lowest intensity considered here, evolving into pure tunneling by saturation. Although Keldysh theory predicts tunneling ionization for all three intensities, the more complete calculations [11] predict that the transition occurs at a slightly higher intensity.

Figure 1 shows the angle resolved PE spectrum (ARPES) for helium at the saturation intensity. Evident is the preponderance of PE energies lying below $2U_p$, which is the upper limit predicted by a simple quasiclassical (SQC) model [3]. The angular distributions (AD) of these electrons are strongly aligned along the laser polarization direction (see polar inset), becoming narrower toward the $2U_p$ limit. However, a striking change occurs in the AD of electrons with energies above $2U_p$. Here the AD's are significantly broader with a weak narrowing as the energy increases toward $10U_p$. In fact, this ARPES seems to be a superposition of two components: a "normal" narrow distribution that falls off rapidly with increasing energy between 0 and $2U_p$, and a much broader but weaker, almost flat energy distribution that extends out to surprisingly high energies before abruptly truncating at $8-10U_p$. This differs dramatically from all previous experimental reports [1]. For example, the PE distributions for inert gas atoms [7,8] clearly show angle-dependent structures, as well as an abundance of electrons with energies $>2U_p$. We show that these differences are due to the pure tunneling nature of the helium ionization at this high saturation intensity.

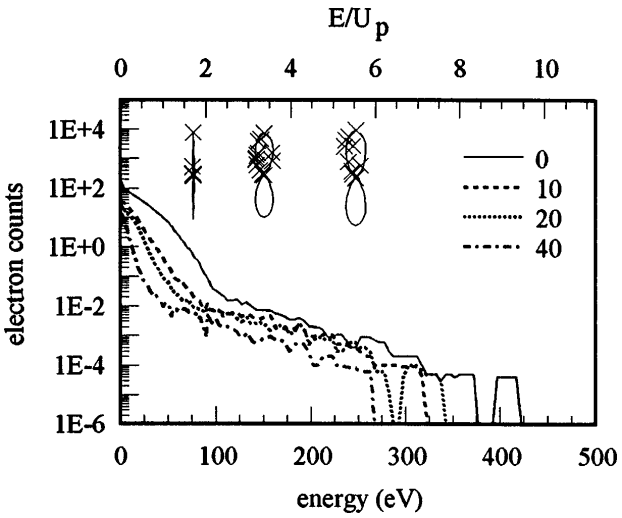

FIG. 1. Measured helium ARPES for four different emission angles at the saturation intensity. The polar plots show the measured ADs (crosses) at the indicated energies and the solid lines are only to guide the reader.

Total PE distributions are obtained by integrating the angular distributions over the polar angle and assuming azimuthal symmetry about the polarization axis. These distributions are shown in Fig. 2 for three different intensities in both absolute and scaled energy units. The distributions are constructed by integrating the experimental ARPES over the polar and azimuthal angles. In absolute units, an increasing laser intensity results in the production of higher energy electrons. However, in energy units scaled to U_p, the PE distributions at all intensities are similar in shape. If these three distributions are scaled such that their low energy maxima are made equal, one sees that the fraction in the high energy plateau drops with increasing intensity, scaling approximately as $I^{-2.5}$. As will be discussed below, all these features result from a consistent and

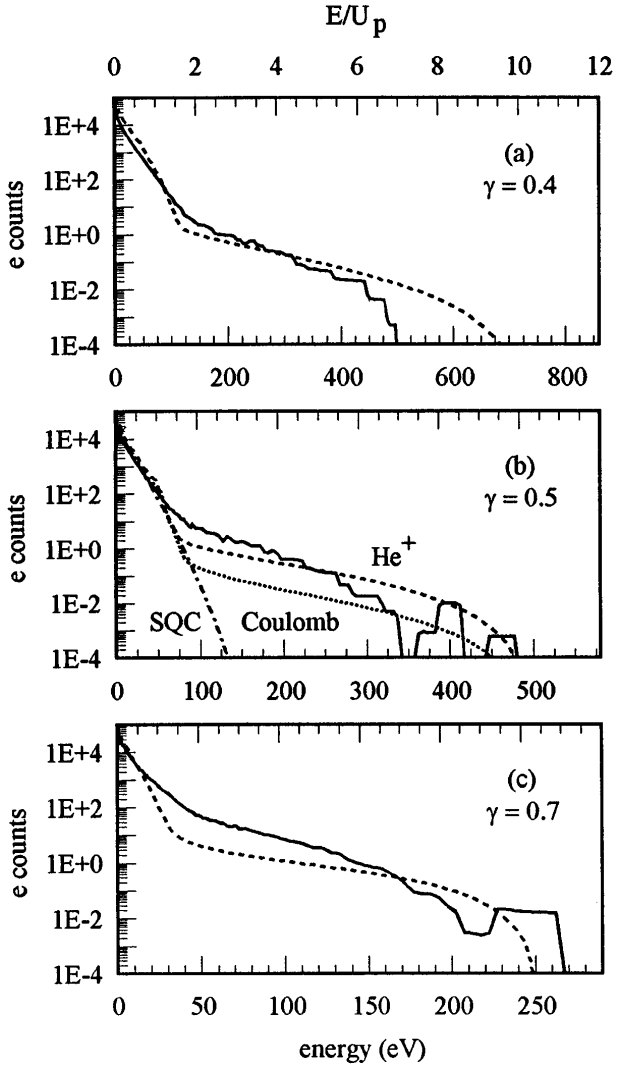

FIG. 2. Total helium PE energy distributions for 780 nm excitation at (a) 12, (b) 8, and (c) 4×10^{14} W/cm^2. The experimental and calculated distributions using the complete semiclassical theory presented here correspond to the solid and dashed lines, respectively. In panel (b) the dotted line results from pure Coulomb rescattering and the dash-dotted is without rescattering (SQC model).

quantitative picture of elastic rescattering of a field–driven electron in the tunneling limit.

The demarcation between the ionization pathways mentioned above becomes apparent when the wave packets promoted from the bound state into the continuum in these two limiting cases are considered. In the MPI regime, ionized population appears continuously, at all phases of the field. To conserve momentum, this transition must take place while the electron is close to the nucleus producing a wave packet, initially localized near the ion core. When the intensity increases to the point that $\gamma < 1$, tunneling begins to dominate and the electron is released a significant distance from the nucleus. During a narrow time interval near the maximum in the oscillating electric field, an asymmetric, delocalized wave packet emerges at the outer edge of the suppressed Coulomb barrier. However, the overall symmetry of the ionization process is maintained by a complementary wave packet being generated on the opposite side of the nucleus one-half cycle later. Clearly, the evolution of the continuum wave packets in these two limiting cases can be very different, which is reflected in our experiment.

The motion of the tunneling wave packet is controlled mostly by its interaction with the laser field since it rapidly moves beyond the range where the ion core potential is effective. Its evolution can be reasonably approximated using the classical equations of motion for a laser–driven electron. In the SQC model [3], the bound electron becomes free at a particular phase, ωt_0, of the field, then undergoes oscillatory motion at the laser frequency, ω. The electron–field interaction in the length gauge can be written as $e\mathcal{E}\hat{z}\sin\omega t$, where $\hat{z}$ is the direction of polarization and $\mathcal{E} = \sqrt{8\pi I/c}$ is the amplitude of the laser's electric field. Assuming that the electron is initially at rest after tunneling, the time dependent electron velocity is given in atomic units as $v(t) = (\mathcal{E}/\omega)(\cos\omega t - \cos\omega t_0)$, where the first term is the field–induced quiver motion and the second term the drift velocity which is established the instant the electron appears in the continuum. In a short pulse experiment, the detected PE energy corresponds to this drift energy. Therefore, in the absence of further interactions with the ion core (rescattering) the maximum drift energy an electron can have is $2U_p$. This is borne out in a SQC calculation of the PE energy distribution which is shown by the dashed-dotted line in Fig. 2(b). The obvious failure of the SQC model in predicting the high energy portion of the spectrum indicates the necessity of including rescattering from the ion core potential in order to reproduce our measured ARPES.

In the tunneling regime electrons released into the field are initially accelerated away from the ion core. Roughly half the electrons will recross the plane of the nucleus when the field has changed sign, having propagated for at least half an optical cycle beyond the range of the ion core potential. During this interval the wave packet will spread freely in the transverse directions. Classical analysis [8,12] shows that PE's with energies $>2U_p$ are produced by trajectories which experience very large deflections (elastic backscattering, $\theta > \pi/2$) when they rescatter from the ion core. The electron's scattering angle and final drift energy are closely correlated. The elastic differential cross section in the backward direction can be approximated by that for Rutherford scattering, $\sigma(\theta) \sim (1/E^2)\csc(\theta/2)$ [13], which varies slowly over the critical angular range, producing the flat energy distribution for these PE's. The hard collisions (small impact parameters) necessary for producing large changes in drift energy also result in the broader angular distributions observed in the high energy electrons.

Our earlier numerical studies on neutral helium found that the returning wave packet at this wavelength has a radius of approximately $30a_0$ as it rescatters from the nucleus. For a given atom this width does not depend on the laser intensity, but only on the free propagation time and therefore only on the laser wavelength. The transverse expansion causes most returning trajectories to have very large impact parameters. This explains the observed small fraction of electrons with energies $>2U_p$ in Figs. 1 and 2.

We can extend the SQC model to include the effect of the first rescattering on the tunneling wave packet. As in the SQC model, we divide the optical cycle into a large number of equal time intervals. In each interval a trajectory is launched at the outer turning point of the suppressed effective potential with zero velocity. It is propagated in the combined fields of the laser and the helium ion core until either it escapes or returns to cross the plane of the nucleus. Those which escape contribute to the spectrum below $2U_p$ according to their drift velocities as in the SQC model. The returning trajectories are assumed to be guiding a freely spreading Gaussian wave packet whose width is given by $\alpha(\tau) = \sqrt{\alpha(0)^2 + [2\tau/\alpha(0)]^2}$, where $\alpha(0)$ is the initial width and τ is the propagation time between initiation and return. Choosing $\alpha(0) = 4.0a_0$ gives a return width consistent with our numerical studies [11]. We calculate the differential elastic scattering cross section for this wave packet using [13]

$$\sigma(\theta) = \left| \frac{1}{2ik} \sum_{\ell=1}^{\ell_{\max}} a_\ell (2\ell + 1) e^{2i(\eta_\ell + \delta_\ell)} P_\ell(\cos\theta) \right|^2 . \quad (1)$$

Here δ_ℓ is the Coulomb phase shift (for a charge of 1) and η_ℓ is the additional phase shift resulting from the short range part of the $\mathbf{He}^+$ potential. These phase shifts are obtained from numerical integration of the scattering equations for electron–$\mathbf{He}^+$ over the necessary range of energies and angular momenta. The partial wave amplitudes a_ℓ are determined from the distribution of impact parameters in the returning wave packet ($\ell = m v_{\text{ret}} b$).

Equation (1) gives the field–free differential cross section. The laser field will distort this distribution. The transverse component of the outgoing velocity is conserved, but the velocity along the polarization direction has both a drift component and a quiver velocity which depend

on the phase of the laser field at the return time. Drift velocities corresponding to PE energies as high as $10U_p$ can be produced if the trajectory is scattered by $\sim 180°$. The energy and angular distributions from the wave packet in each time interval are weighted by the instantaneous tunneling rate. In these calculations we have actually used a scaled dc-tunneling rate which, when cycle averaged, gives the ADK rate [14]. This accounts for the initial state not being purely hydrogenic. The total ARPES for a given laser intensity is obtained by summing the contributions from all time intervals.

Spatial and temporal averaging provides the total PE spectrum shown by the dashed lines in Fig. 2. The agreement with the experimental results is excellent over the entire energy range for both "pure" tunneling cases. The poorer agreement seen in Fig. 2(c) signifies the transition into the mixed regime where the MPI contribution is becoming significant. In fact, because of the low intensity contributions to the measured PE signal from the outer regions of the focal volume, there are "MP" components to all three cases shown. However, the strong intensity dependence of the ionization rate means the fractional contribution of these electrons to the total yield is small and decreases with intensity, and they will appear within the lower energy portion of the spectrum. This may account in part for some of the disagreement between the calculations and the measurements for lower PE energies. Finally, Fig. 2(b) also shows a PES calculated using a pure hydrogenic potential. This significantly underestimates the high energy plateau because the backscattering which produces the high energy electrons is most strongly affected by the more attractive short range part of the real potential.

These calculations also provide the ARPES which we show for I_{sat} in Fig. 3. The calculated results are much smoother than the measured values (Fig. 1), but reproduce the angle-dependent cutoffs in energy and the flatness of the high energy component. We obtain similarly good agreement for the other intensities studied except that at the highest intensity the measured PE spectrum ends around 10–20% lower energy than we predict. This may be due to poorer statistics in the measurement for the most energetic electrons at the highest intensity.

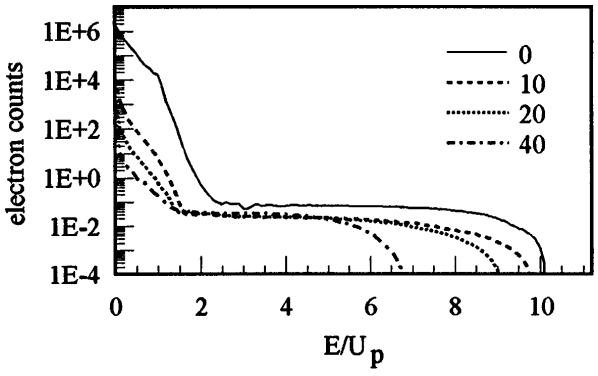

FIG. 3. Calculated helium ARPES for four different emission angles at the saturation intensity of a 150 fs, 780 nm laser from full semiclassical theory. The results are presented incorporating the experimental geometry.

In this Letter we have presented the first careful study of PE distributions obtained in the tunneling regime. The distinctive energy and angular distributions are shown to be a clear signature of this limit. We showed that we could quantitatively reproduce these spectra using a more complete quasiclassical model which includes the effects of recollisions with the ion core. Our calculation ignores higher order rescattering processes which we believe are much less significant because the continuing transverse spreading rapidly diminishing the effect of further interactions with the nucleus. If these subsequent collisions were important, the comparison between the measured and calculated spectra would be much less favorable. The characteristics of the ARPES, the flat distribution above $2U_p$, and especially the well defined angle and energy cutoffs, strongly support the tunneling wave packet picture. Our analysis shows that the strength of the high energy plateau is sensitive to the initial width of the tunneling wave packet. The agreement we have obtained supports the value we have determined and probably rules out anything substantially different from this. We note also that the previous quasiclassical studies by Lewenstein *et al.* [12] give qualitative agreement with our new measurements, but are not at all quantitative for any reasonable set of input parameters. This is possibly in part due to approximations used in modeling the ion core potential.

We gratefully acknowledge the technical assistance of Robert Lafon, Mark Widmer, and Alok Gambhir. This research was carried out in part at Brookhaven National Laboratory under Contract No. DE-AC02-76CH00016 with the U.S. Department of Energy and supported by its Division of Chemical Sciences, Office of Basic Energy Sciences, and in part under the auspices of the U. S. Department of Energy at the Lawrence Livermore National Laboratory under Contract No. W-7405-ENG-48.

[1] For a review, see L. F. DiMauro and P. Agostini, in *Advances in Atomic, Molecular, and Optical Physics 35*, edited by B. Bederson and H. Walther (Academic Press, San Diego, 1995).
[2] L. V. Keldysh, Sov. Phys. JETP **20**, 1307 (1965).
[3] P. B. Corkum *et al.*, Phys. Rev. Lett. **62**, 1259 (1989).
[4] S. Augst *et al.*, J. Opt. Soc. Am. B **8**, 858 (1991).
[5] T. Auguste *et al.*, J. Phys. B **25**, 4181 (1992).
[6] U. Mohideen *et al.*, Phys. Rev. Lett. **71**, 509 (1993).
[7] Baorui Yang *et al.*, Phys. Rev. Lett. **71**, 3770 (1993).
[8] G. G. Paulus *et al.*, J. Phys. B **27**, L703 (1994).
[9] K. J. Schafer *et al.*, Phys. Rev. Lett. **70**, 1599 (1993).
[10] P. B. Corkum, Phys. Rev. Lett. **71**, 1994 (1993).
[11] B. Walker *et al.*, Phys. Rev. Lett. **73**, 1227 (1994).
[12] M. Lewenstein *et al.*, Phys. Rev. **51**, 1495 (1995).
[13] L. I. Schiff, *Quantum Mechanics*, 3rd ed. (McGraw-Hill, New York, 1968).
[14] M. V. Ammosov, N. B. Delone, and V. P. Krainov, Sov. Phys. JETP **64**, 1191 (1986).